ACS Sustainable Chemistry & Engineering

pubs.acs.org/journal/ascecg

Research Article

Artificial Coal: Facile and Green Production Method via Low-Temperature Hydrothermal Carbonization of Lignocellulose

Zhi-Xiang Xu,* Xue-Qin Ma, Ya-Qi Shan, Xun Hu, Sameh M. Osman, Jun-Jie Liao, Pei-Gao Duan,* and Rafael Luque*

Cite This: *ACS Sustainable Chem. Eng.* 2022, 10, 3335−3345

Read Online

ACCESS | Metrics & More | Article Recommendations | Supporting Information

ABSTRACT: A new concept is proposed for the production of artificial coal under HTC conditions using $Mg(NO_3)_2$ as an oxidant in a short time, which is found to enhance the coalification degree of hydrochar from lignocellulosic materials. Pressure promotes decarboxylation reactions of lignocellulose to form hollow smooth-faced regular spherical particles, avoiding the agglomeration of hydrochar particles. In parallel, oxidation can break down the biopolymer structure to form low-molecular-weight compounds, which is found to be a key step during artificial coal formation. The artificial coal synthesized has a high degree of coalification.

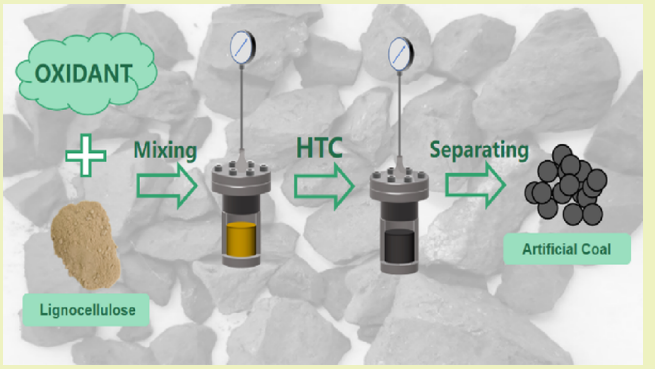

KEYWORDS: *carbon neutrality, artificial coal, hydrothermal carbonization, pressure, mechanism*

1. INTRODUCTION

The population expansion and increasing industrialization and urbanization call for a growing fossil fuel energy demand, which simultaneously leads to serious water and soil pollution and climate changes.[1] Although various clean energies are developed after Paris Agreement,[2] fossil fuels are the dominant energy supplier worldwide including 27% of coal, 33.1% of oil, and 24.2% of natural gas.[3] Accordingly, developing clean energy generation from waste organic material to reduce CO_2 emissions is of great interest to researchers.[4] Hydrothermal carbonization (HTC) first reported by Bergius as early as 1913[5] is a thermal treatment of biomass in an aqueous medium heated at subcritical temperatures (180−260 °C) under self-generated pressure (0−2 MPa) to obtain solid char.[6] HTC has been extensively investigated to mimic the natural process of coal formation.[7] The past two decades have seen a renewed interest in the topic due to its green technology.[8] The main advantage of HTC is that biomass does not require a preliminary drying step since it is a process taking place in water, which subsequently saves significant amounts of energy especially high-moisture waste including food waste, sewage sludge (SS), livestock manures, and others.[9,10] On the other hand, it can also provide a low coalification degree of solid fuel to replace coal.

During HTC of lignocellulose, dehydration, polymerization, and aromatization reactions occur with the condensed polyfuranic system bridged by aliphatic regions and terminal hydroxyl and carbonyl functional groups formed.[11] Lignin is only a marginally altered fraction in the HTC process, which affects the final hydrochar structure as it interferes with cellulose hydrolysis, resulting in a rather challenging cellulose conversion.[12,13] Conversely, converting lignocellulosic biomass into carbonaceous materials with the same chemical structure and morphology is still a highly challenging task.[11,14] Besides lignocellulose, livestock manure, SS, and food waste also contain proteins prone to deamination to form heterocyclic compounds during HTC.[15] Hydrochar from lignocellulose has been proved to possess a relatively low degree of coalification (in the region of lignite in the Van Krevelen diagram).[16,17] Improving hydrochar properties at relatively low temperature is a key step to realize the HTC-to-artificial coal concept, especially as alternative natural coal. A feasible pathway to convert lignocellulose during HTC is to form polyfuranic chains as a key step to lignocellulose conversion during HTC and following arene formation under harsh reaction conditions.[18,19] However, arene formation is relatively difficult under low-temperature HTC conditions, even with a strong acid as a catalyst.[20,21]

Received: December 11, 2021
Revised: January 5, 2022
Published: February 28, 2022

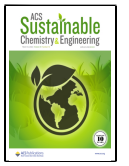

Simulation coalification experiments have been carried out from peat, wood, or others in recent decades, mainly considering temperature and pressure with organic geochemical analyses. However, the required harsh conditions (408 atm, 125 °C, 75 days) as well as long reaction times make artificial coal preparation a highly challenging task.[22,23] Under conventional HTC temperatures and pressures, lignin is relatively stable.[12,17] The main change in lignin structure is the cleavage of carbon side-chain moieties as well as demethylation, causing an increase in catechol-like structures.[12,24] Proteins are also difficult to be incorporated into the hydrochar as they undergo deamination and decarboxylation.[25,26] Under conventional HTC conditions, another challenge of cellulose, lignin, and proteins is the low hydrolysis rate, resulting in a large amount of feedstock directly transferred to hydrochar, essentially leading to a low degree of carbonization in the hydrochar itself.

To fill the existing gap on artificial coal preparation, this contribution reports an unprecedented, flexible, simple, and reproducible method to enhance the coalification degree of hydrochars from HTC of lignocellulosic feedstocks mediated by the addition of an oxidant to disrupt the polymeric structure (enhancing hydrolysis). Cellulose (CL) and lignin (LG) were used as single-component model compounds. Egg white powder (EWP) was used as a protein model with a polysaccharide mixture. Pine wood powder (PWP) was used as a natural lignocellulose compound. Specifically, the objectives of this research were to (i) characterize the hydrochar generated under partial oxidation conditions, (ii) characterize the influence of the partial oxidation atmosphere, and (iii) assess the potential influence of reaction pathways.

2. MATERIALS AND METHODS

2.1. Materials. CL and LG were supplied by Shanghai Macklin Biochemical Co. Ltd. PWP and EWP were directly derived from the market and pulverized to below 150 μm. $Mg(NO_3)_2$ (MN) and $K_2S_2O_8$ (KS) were AR and used without further purification.

2.2. HTC Experiments. Five grams of the sample, 5 g of oxide, and 70 mL of distilled water were used for HTC in a 100 mL autoclave reactor (Nanjing Zhengxin Instrument Co. Ltd., Nanjing, China). The withstand pressure value was 25 MPa at 340 °C. Upon quantification, samples were directly poured into the reactor and mixed under magnetic stirring. The reactor was then sealed and heated to the setting temperature by an electrical heater that was held for the setting time when the temperature reached the setting value. If the reaction time was completed, the reactor would stop heating and cool to room temperature. The mixture was directly filtered with a vacuum pump to separate the solid and liquid. The solid was rinsed with distilled water and then heated at a 105 °C oven for 24 h to obtain a solid.

To analyze the influence of pressure on hydrochar properties during HTC, 5 g of sample, 5 g of oxide, and 40 mL of distilled water were added into a 100 mL autoclave reactor together with nitrogen gas (ps-100, Nanjing Zhengxin Instrument Co. Ltd., Nanjing, China). The maximum values of temperature and pressure were 340 °C and 40 MPa, respectively. After sealing, the N_2 steel cylinder was opened and released nitrogen entered the force lift pump (JTT40, Jackatech Fluid Equipment Manufacturing Plant, Jining, Shandong, China) to increase pressure. After reaching the setting value, the force lift pump, N_2 steel cylinder, and reactor were closed sequentially. The other process was the same as that without N_2. The hydrochar samples under different conditions are listed in Table S1.

2.3. Materials Characterizations. The elemental compositions of the hydrochars were analyzed by an elemental analyzer (Flash2000 CHNS/O, Thermo Fisher Scientific, USA). Oxygen content in hydrochar was also measured with this instrument. Fourier transform infrared spectroscopy (FTIR) analysis of the hydrochars was performed by a VERTEX 70 FTIR spectrometer (Bruker, Germany). The conditions of thermogravimetric analysis (TG) (STA449F5, NETZSCH, Germany) were as follows: about 10 mg of hydrochar, a heating rate of 10 °C/min, from room temperature to 900 °C, and a constant flow of N_2 at 40 mL/min. An X-ray diffraction (XRD) spectrometer was used to analyze the crystallinity of the hydrochars (D8 Advance, Bruker, Germany). A Cu target (Cu Kα source) was used and the scanning rate was 20°/min from 5° to 90°. X-ray photoelectron spectroscopy (XPS, Thermo ESCALAB 250 instrument) was employed to probe organic N and C functional groups on the surface of the hydrochars. A monochromatized Al Kα source (1486.68 eV) was used to obtain the spectra. The voltage was 14.8 kV, the current was 1.6 A, and the power was 150 W. The spectra were corrected by C 1s (284.8 eV). The spot diameter was 650 nm. The morphology was observed by scanning electron microscopy (SEM, Merlin, Zeiss). Raman measurements were performed on a LabRAM HR Evolution (Renishaw inVia, England) with a laser wavelength of 532 nm to analyze the carbonization degree of N-hydrochar. Nuclear magnetic resonance (NMR) analysis including ^{1}H NMR and ^{13}C NMR spectroscopy (400 MHz, Bruker AVANCE III 600M) was carried out to analyze the properties of carbon-containing functional groups and hydrogen-containing functional groups ascribed to the surface of N-hydrochar. The specific surface area was tested by N_2 adsorption using a physisorption analyzer (Kubo-X1000, Beijing Builder Optics Co. Ltd.). Particle size was measured by a Mastersizer 2000 (Malvern PANalytical, England). A gas chromatography−mass spectrometer with an HP-5MS column (30 m × 0.32 mm × 0.25 mm) was used to analyze the oil components in the aqueous phase by a Thermo Trace1300, ISQ 7000, USA. The total organic carbon (TOC) of the aqueous phase was measured by a Shimadzu TOC-VCSH analyzer (Shimadzu, Japan).

3. RESULTS AND DISCUSSION

3.1. Hydrochar and Aqueous Phase Characteristic Analysis. Table S2 summarizes the elemental analysis results for hydrochars produced with different feedstocks under different conditions. Compared to pure CL at 260 °C, the content of hydrogen, oxygen, and carbon in hydrochar with MN decreased from 4.44 to 3.63%, from 30.25 to 22.98%, and from 68.61 to 65.68%, respectively, under identical temperatures and reaction times. H/C and O/C values notably decreased, indicating that MN can significantly promote dehydration and decarboxylation to enhance the degree of carbonization. The content of carbon and hydrogen notably decreased (especially carbon) at 300 °C, while the content of oxygen increased. The carbon content decrease was probably related to thermal decomposition of oligomers to form low-molecular-weight compounds (or oligomers were deeply oxidized to form gases). The oxygen content increased probably due to thermal decomposition of oligomers and formation of more carboxylic acid functional groups on the surface. Larger amounts of carbon were oxidized at prolonged times of reaction (10 h, 260 °C), with similar results to those observed at 300 °C. Comparatively, the addition of KS brought a slight reduction of carbon and hydrogen content while the oxygen content notably decreased. Compared to hydrochar with KS, hydrochar with MN at 260 °C has lower hydrogen and oxygen content, especially hydrogen, indicating that MN has a stronger role in disrupting the CL structure, with improved dehydration and decarboxylation capability as compared to KS.

The use of LG and EWP provided similar results, with the exception of a stronger decarboxylation capability of KS (as compared to MN), probably related to the chemical structure of the feedstock. When PWP was used as a feedstock, similar

https://doi.org/10.1021/acssuschemeng.1c08338
ACS Sustainable Chem. Eng. 2022, 10, 3335−3345

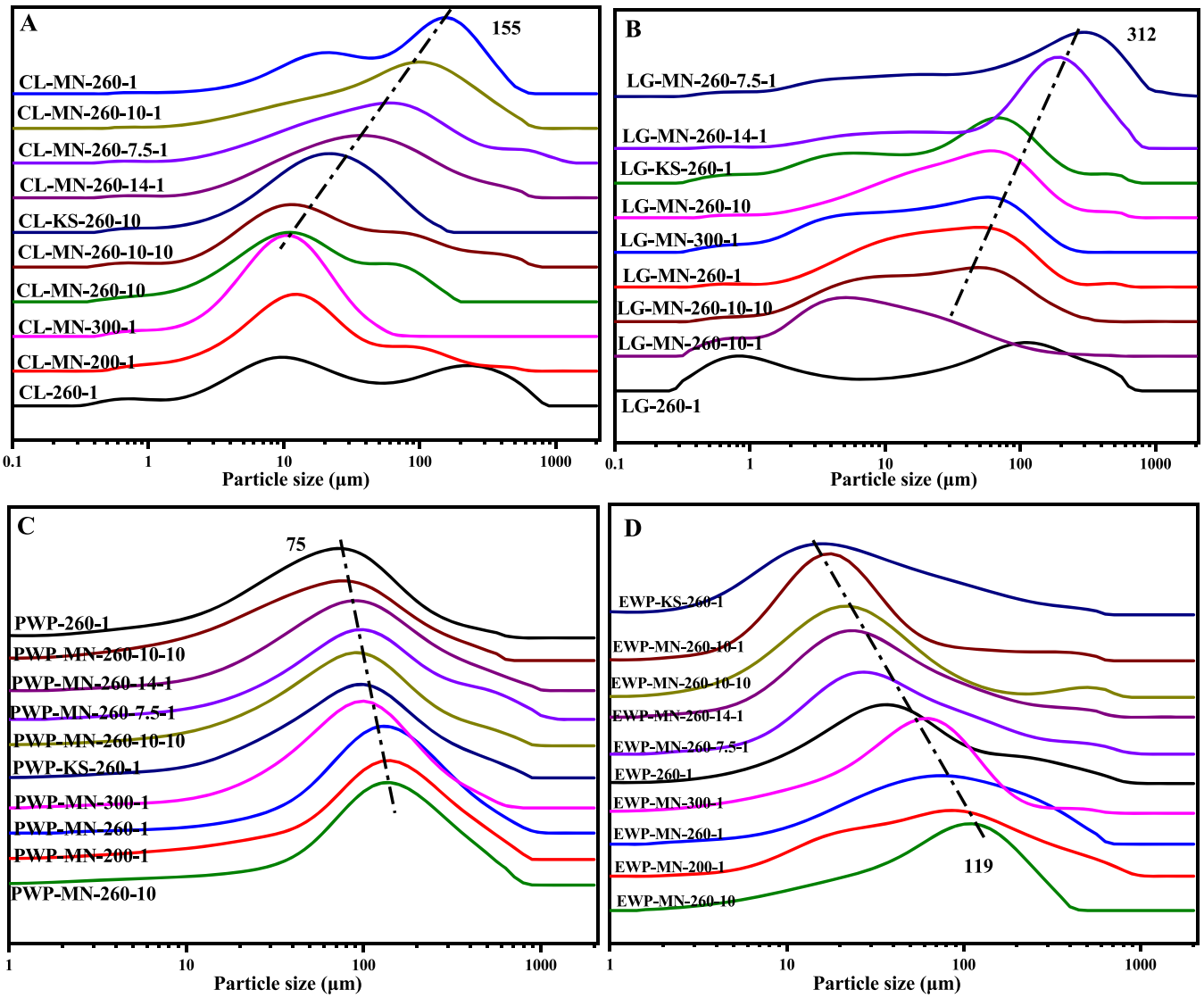

Figure 1. Particle size of hydrochar. (A) Particle size of CL-derived hydrochar; (B) particle size of LG-derived hydrochar; (C) particle size of PWP-derived hydrochar; (D) particle size of EWP-derived hydrochar.

results were also found, but the content of carbon, hydrogen, and oxygen in PWP-derived hydrochar was comparatively higher than that of CL-derived hydrochar. These indicated that the interaction between LG and CL influenced hydrochar formation, in agreement with a previous report.[13] According to elemental analysis results, the presence of an oxidant and pressure played important roles during HTC.

To further ascertain the role of partial oxidation during HTC, the Van Krevelen diagram for hydrochars is depicted in Figure S1. Most samples were close to the coal region. H/C values were lower than that of conventional HTC for biomass.[14] Most hydrochar characteristics were close to those of lignite during HTC after just 1 h. O/C values were very high, particularly for LG and CL at 300 °C (1 h) and 260 °C (10 h), indicating that LG and CL underwent partial decomposition and oxidation to −COOH groups that account for the increased oxygen content listed in Table S2. H/C values notably decreased, indicating that partial oxidation promoted hydrochar coalification at the same HTC temperature and reaction time.

Lower O/C values were present in EWP-derived hydrochar, pointing to a different reaction mechanism or a favored decarboxylation (to form and remove CO_2) as compared to CL and LG (Figure S2). The increasing pressure value in the systems led to hydrochars also within (or close) the coal range, with H/C and O/C shifted to lower values, confirming the coalification promotion of hydrochar.

To further analyze hydrochar properties, FTIR results are also compiled in Figure S3. Strong C═C vibrations and weak C═O vibrations could be found for the use of CL as a feedstock with MN at 260 °C, indicating that MN promoted C═C formation.[27] C═O bands almost disappeared at 300 °C (or 260 °C for 10 h), pointing to enhanced decarboxylation. C−H vibrations located at 880 and 740 cm^{-1}, corresponding to out-of-plane bending vibrations of aromatic groups, could also be observed, indicating that the degree of carbonization notably increased (no bands located in this region during conventional HTC using CL as a feedstock).[28]

Partial oxidation (same results observed for KS) consequently had a positive effect in the HTC of CL. C═O almost disappeared (and C−H vibration bands located at 880

https://doi.org/10.1021/acssuschemeng.1c08338
ACS Sustainable Chem. Eng. 2022, 10, 3335−3345

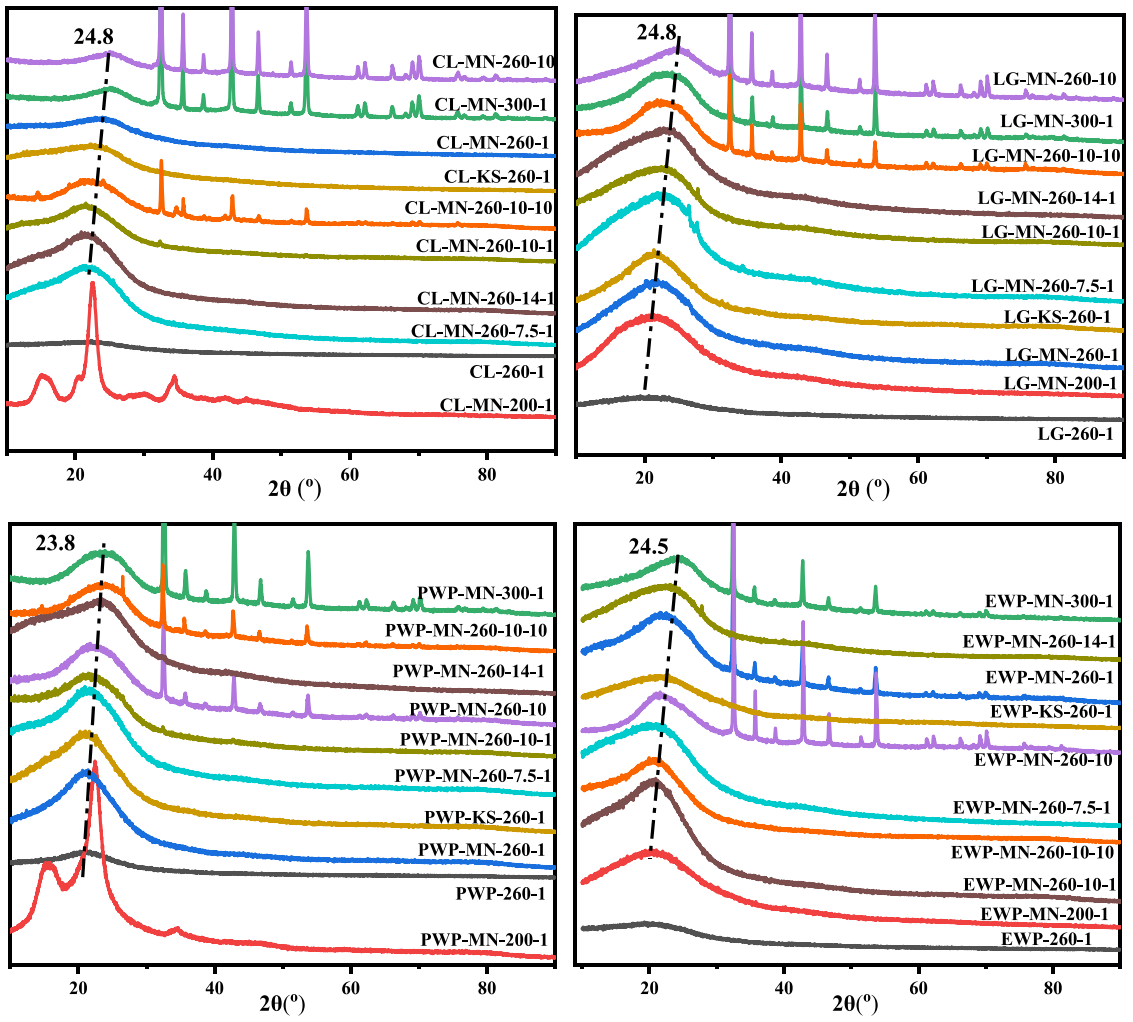

Figure 2. XRD results of hydrochar. (A) Particle size of CL-derived hydrochar; (B) particle size of LG-derived hydrochar; (C) particle size of PWP-derived hydrochar; (D) particle size of EWP-derived hydrochar.

and 740 cm^{-1} appeared) when pressure was applied (10 MPa), indicating that decarboxylation was enhanced. No C═O peak could be found at lower temperatures (200 °C), pointing to the formation of C═O after hydrolysis.

When LG, PWP, and EWP were employed as a feedstock, similar results were also found. PWP-derived hydrochar prepared under pressured conditions showed almost non-existent C═O bands, implying that pressure was beneficial to remove CO_2. FTIR results further confirmed the influence of pressure on the degree of decarboxylation. Comparably, the added oxidant could disrupt the organic matter to enhance hydrolysis and positively influenced the hydrochar formation process, in good agreement with previous results.[22]

To further analyze the hydrochar properties, particle size was further characterized. Results are listed in Figure 1. When CL was used as a feedstock, two main peaks appeared (9.8 and 275 μm) at 260 °C, which was held for 1 h, indicating that part of cellulose was directly converted to a solid during HTC. A pyrolytic pathway during HTC for cellobiosan appeared even at 260 °C.[29] Similar results could be found for the addition of MN, with a weakened peak (10 μm) and the disappearance of the peak at 275 μm. These results pointed to an enhanced hydrolysis of unreacted CL. When the reaction was prolonged to 10 h, two peaks could still be found (80 μm was weak), while only one peak could be found at ca. 10 μm at 300 °C (same results observed with pressure increasing). The results pointed out the incomplete hydrolysis of CL. From particle size results, the presence of an oxidant and pressure promoted the hydrolysis to inhibit solid-to-solid conversion, but CL was still not completely hydrolyzed. Similarly, the use of MN as an oxidant promoted lignin hydrolysis to inhibit the solid-to-solid reaction when LG was used as a feedstock as compared to the reaction conducted in the absence of an oxidant (two main peaks appeared at ca. 1 and 110 μm, indicating that a small part of lignin hydrolyzed and then polymerized to hydrochar; a large amount of lignin was directly converted to a solid during HTC). MN changed the surface characteristics of the samples and the morphology and contributed to particle aggregation. Similar results were observed for the use of EWP as a feedstock (Figure 1). HTC properties of EWP were different from those of CL and LG. When PWP was used as a feedstock under 260 °C without oxide, it was found that the particle size reached near 70 μm. When oxide was added under the same HTC condition, the particle size shifted to a high value. PWP containing cellulose and lignin, which interfere with cellulose hydrolysis,[30] was not completely hydrolyzed. When oxide was added, more hydrolysates could still be obtained on the surface of the residue to form bigger particle sizes in the hydrochar. Under harsher reaction conditions, the particle size became

https://doi.org/10.1021/acssuschemeng.1c08338
ACS Sustainable Chem. Eng. 2022, 10, 3335−3345

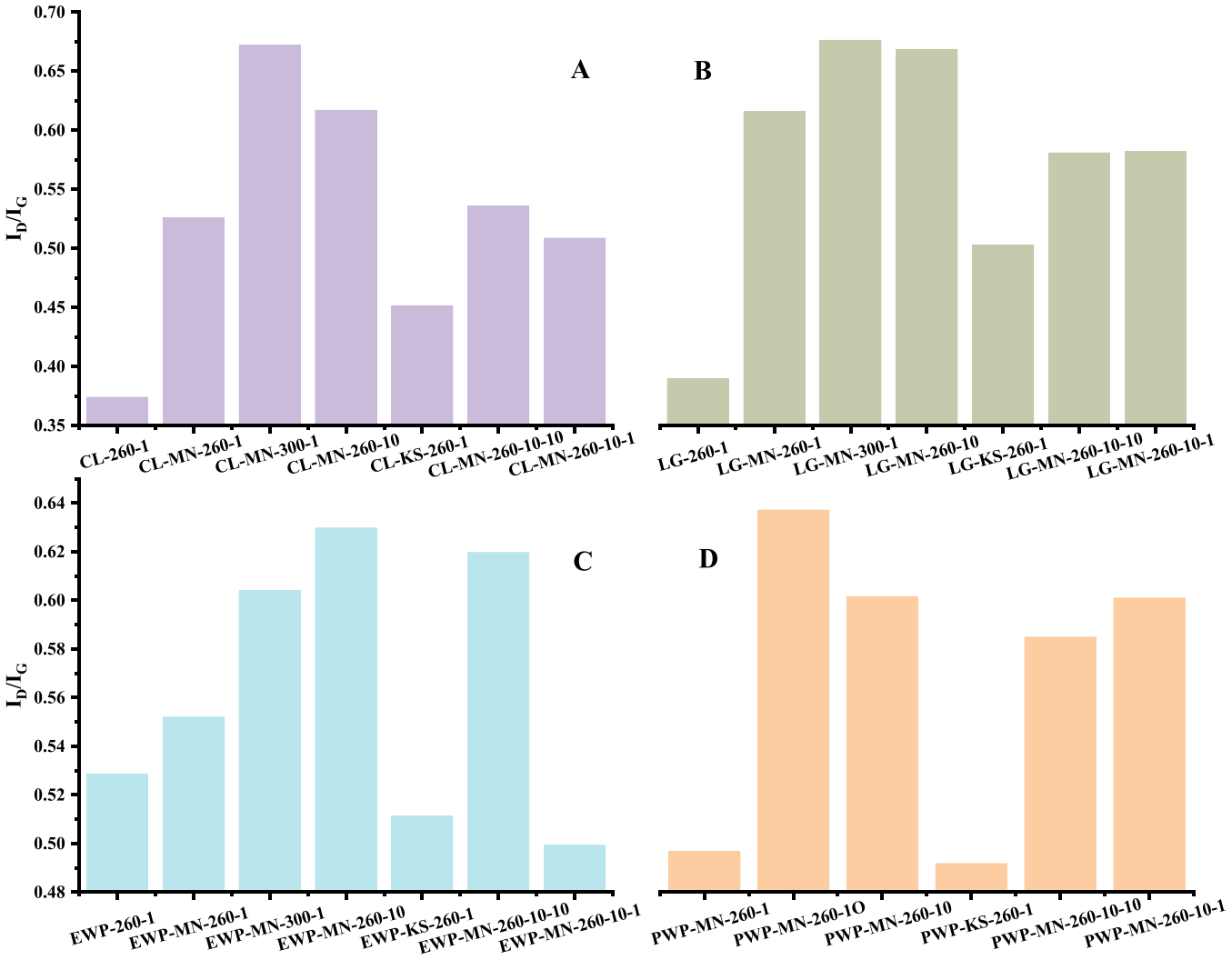

Figure 3. I_D/I_G results for Raman spectrum of hydrochar under different conditions. (A) CL-derived hydrochar; (B) LG-derived hydrochar; (C) PWP-derived hydrochar; (D) EWP-derived hydrochar.

smaller, indicating that thermal decomposition and hydrolysis were enhanced to weaken the formation of aggregates.

To further analyze the characteristics of the synthesized hydrochars, XRD was employed as depicted in Figure 2. When CL was used as a feedstock, the hydrochar has a high carbonization degree at 300 and 260 °C for 10 h. The peak showed a broader peak at 2θ = 24.8°, corresponding to the plane of (002) particularly for diffraction peaks of carbon.[31] In the absence of MN, even at 260 °C, almost no peak could be found. The addition of nitrogen changes the peak at 21.7°, indicating that changes in surface charge were key influences on particle properties.[32] A series of peaks were present (32.5°, 35.6°, 42.6°, 46.6°, and 53.7°) at high temperatures (with pressure) and also with the addition of MN, corresponding to the formation of $MgCO_3$.[33] These pointed out that decarboxylation was enhanced in the presence of MN, in good agreement with elemental analysis results, being also direct evidence of decarboxylation happening during HTC. The same trend was observed for all feedstocks (CL, LG, EWP, and PWP). Ash yield can be used to evaluate the carbonization degree for deep carbonization to form −COOH on the surface, and then it can further form $MgCO_3$. To demonstrate the adsorption of $MgCO_3$ on the surface of hydrochar, the peak of $MgCO_3$ disappeared (Figure S4) after 3.4% dilute HCl solution rinsing. The hydrochar featured an amorphous carbon phase under mild conditions, while under harsher reaction conditions, including higher temperatures, the addition of pressure and the presence of an oxidant could lead to the deep coalification of hydrochar.

To further analyze the degree of coalification for hydrochar, the Raman spectra were also recorded as shown in Figure S5. Two obvious bands could be observed at 1360 and 1590 cm^{-1}, which represented defects and disordered sp^3 carbon (D band) and ordered sp^2 hybridized carbons (G band), respectively.[34,35] The peaks were relatively weak under mild conditions, while they were sharp under harsher reaction conditions. I_D/I_G values, accounting for the degree of defects and disorder of carbonaceous materials, are depicted in Figure 3. I_D/I_G values were low (even at 260 °C) in the absence of MN, under pressure, or at higher temperatures. However, the addition of MN, even at lower temperatures, notably increased I_D/I_G values, indicating a high degree of coalification. Similar results were obtained for all feedstocks, pointing to a universal method to improve the degree of coalification in carbonaceous materials. According to I_D/I_G values, MN has a stronger

https://doi.org/10.1021/acssuschemeng.1c08338
ACS Sustainable Chem. Eng. 2022, 10, 3335−3345

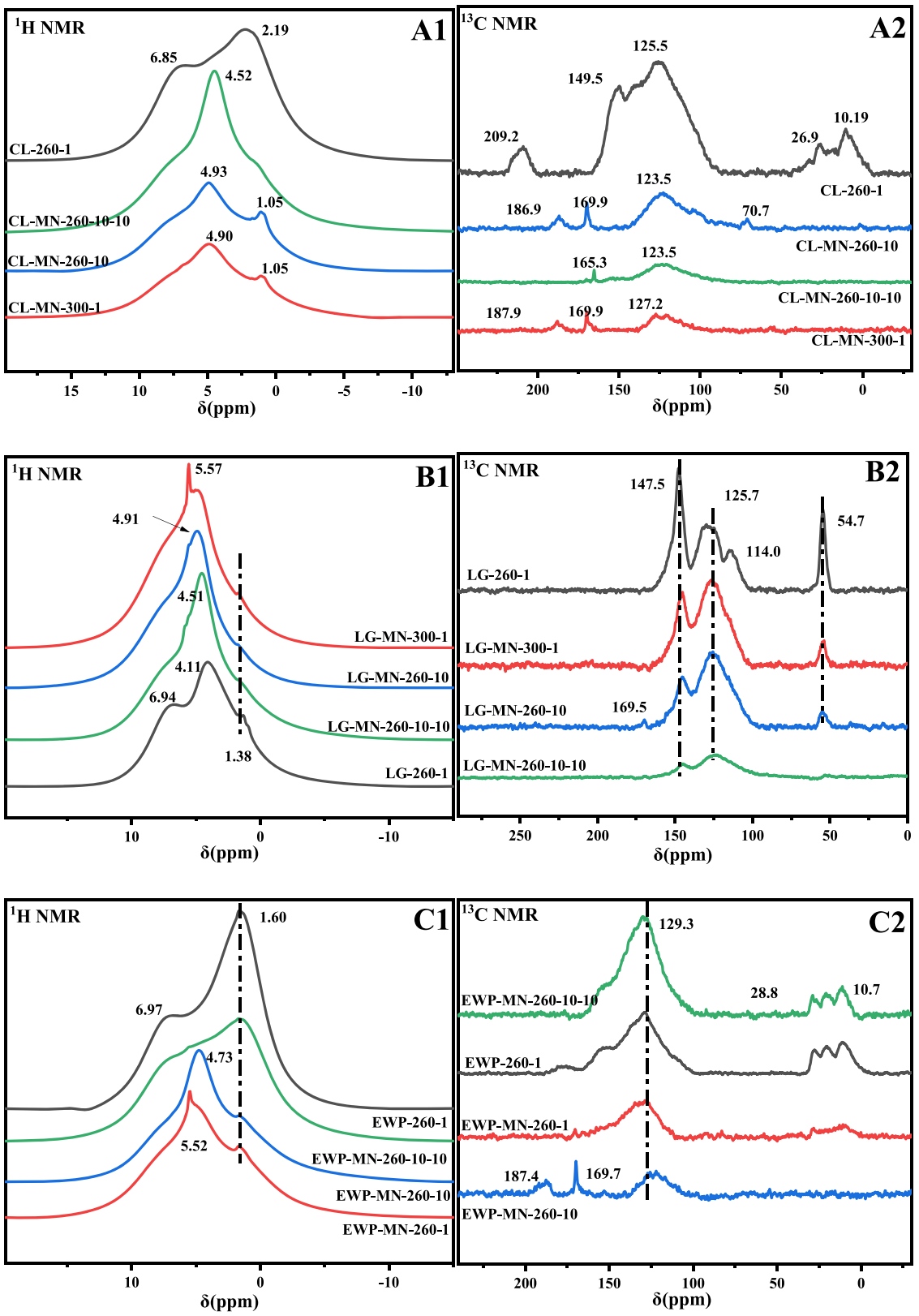

Figure 4. NMR of hydrochar with different conditions. (A) NMR of CL-derived hydrochar; (B) particle size of LG-derived hydrochar; (C) NMR of EWP-derived hydrochar.

capability to improve the degree of coalification as compared to KS.

TG-DTG also was employed to analyze hydrochar thermal decomposition characteristics as summarized in Figure S6. In CL-derived hydrochar, it was found that even at 260 °C, without MN, the thermal decomposition temperature was in the range of 300−600 °C. When MN was added, the initial thermal decomposition temperature of hydrochar shifted to a

https://doi.org/10.1021/acssuschemeng.1c08338
ACS Sustainable Chem. Eng. 2022, 10, 3335−3345

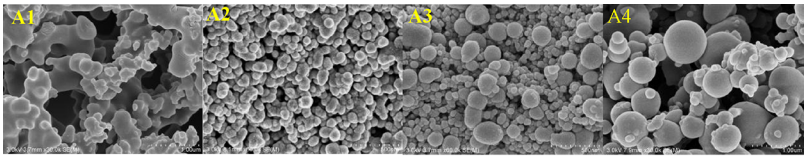

A1:CL-260-1;A2:CL-MN-260-1; A3:CL-MN-260-10; A4:CL-MN-260-10-10

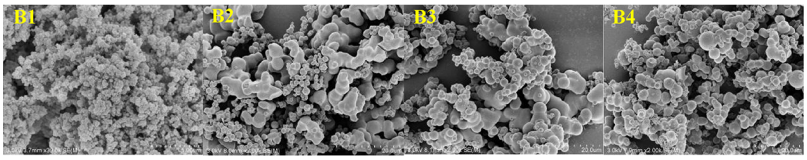

B1: LG-260-1; B2: LG-MN-260-1; B3: LG-MN-260-10; B4: LG-MN-260-10-10

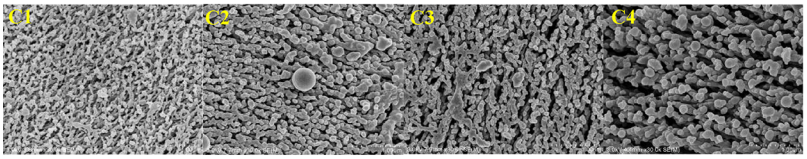

C1: PWP-260-1; C2:PWP-MN-260-1; C3: PWP-MN-260-10;C4: PWP-MN-260-10-10;

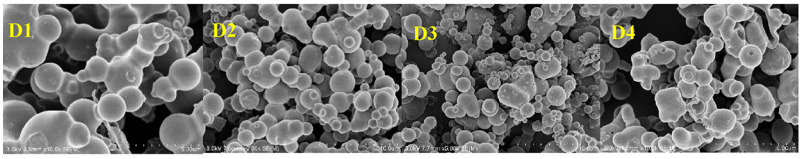

D1: EWP-260-1; D2: EWP-MN-260-1; D3: EWP-MN-260-10; D4: EWP-MN-260-10-10

Figure 5. SEM of hydrochar under different conditions. (A) Particle size of CL-derived hydrochar; (B) particle size of LG-derived hydrochar; (C) particle size of PWP-derived hydrochar; (D) particle size of EWP-derived hydrochar.

high temperature, indicating that the coalification degree of CL was enhanced for thermal decomposition of fixed carbon, which needed a much higher temperature.[36] With the reaction condition changed rigorously, the peak temperature shifted to a high temperature, especially at 260 °C for 10 h having the highest peak temperature. The thermal decomposition temperature of hydrochar exceeded that of some low-rank coals, especially with MN and at 260 °C for 10 h.[37] When LG was used as a feedstock, probably for hydrolysis insufficiency, the peak was split. The highest peak temperature among LG-derived hydrochar was 200 °C. Under harsher conditions, the peak temperature shifted to a low temperature, indicating that CL-derived hydrochar formed hydrochar by polymerization, while the LG structure cleaved by MN decreased the peak temperature. The thermal decomposition temperature of LG-derived hydrochar exceeded that of pure LG.[38] Similar results were obtained for EWP and PWP, pointing to the expected thermal decomposition during HTC. Altogether, a high coalification degree changed the peak temperature.

^{13}C NMR and ^{1}H NMR were subsequently carried out as depicted in Figure 4. In ^{1}H NMR of CL-derived hydrochar, the main peaks were at 6.85 and 2.19 ppm (aromatic protons and O-alkyl protons, respectively).[39] When the reaction condition was at 300 °C (or 260 °C after 10 h), a weak peak located at 1.05 ppm was present due to aliphatic groups. The main peak was located at 4.90 ppm including a weak peak located at 6.85 ppm, corresponding to polyfurfural rings.[17,18] ^{13}C NMR results confirmed that the furanic (C═C—O) peak located at 110–100 ppm was very weak, while the arene (Ar—C═C—Ar) peak was very strong (ca. 127 ppm).[18] These results indicated that the degree of carbonization of the hydrochars was very high. Sharp peaks (125.5 and 149.5 ppm), characteristic of sp^2 carbon atoms in C═C with a signal in the region of 140–160 ppm,[40] can also be found. In the range of 250–150 ppm, a peak located at 209.2 ppm was present, corresponding to the fraction of C═O groups in carboxylic acids (175 ppm), ketones, or aldehydes (200–220 ppm).[41] In the range of 70–0 ppm, the peak in the range of 30–5 ppm corresponded to the aliphatic region.[17] The addition of MN changed the signal profile, with signals present at 70.7 ppm (aliphatic groups) and 186.9 ppm (weak, C═O group in carboxylic acids). Under pressure (10 MPa), peaks (70.7 and 186.9 ppm) disappeared, indicating that decarboxylation was enhanced. A temperature increase to 300 °C only showed a residual peak at 187.9 ppm. Almost no C═O peaks can be found for the use of LG as a feedstock. Two main peaks located at 125.7 and 147.5 ppm could be found, ascribing to aromatic C═C and aromatic carbon bound to lignin methoxy groups, respectively, indicating a condensed aromatic system bridged by aliphatic regions. The peak located at 57 ppm belonged to methoxy groups. In ^{1}H NMR, the main peak located near 5 ppm matched ^{13}C NMR results, being similar to that of CL-derived hydrochar ^{1}H NMR results. A sharp peak located at 1.60 ppm could be found in ^{1}H NMR of EWP-derived hydrochar obtained at 260 °C without MN, ascribing to aliphatic groups. When MN was added, this peak weakened, indicating that MN notably promoted hydrolysis or decomposition during HTC. Another sharp peak was present near 5 ppm, indicating the formation of C═C. In ^{13}C NMR, the main peak located at 129 ppm pointed to polyaromatic ring (including pyrrole pyridine) formation. Polyaromatic rings bridged by aliphatic regions and carbonyl functional groups were formed during HTC. According to NMR results, MN can notably promote coalification while pressure promoted decarboxylation, in

https://doi.org/10.1021/acssuschemeng.1c08338
ACS Sustainable Chem. Eng. 2022, 10, 3335−3345

good agreement with elemental analysis, FTIR, and Raman results.

Specific surface areas (S_{BET}) of hydrochars were also measured as presented in Figure S7. CL- and LG-derived hydrochars exhibited higher surface areas as compared to those obtained from EWP and PWP. CL-derived hydrochar S_{BET} results showed stepwise increment under harsher conditions, indicating that dehydration and decarboxylation were further enhanced to disrupt the agglomeration structure of hydrochar.[42] Pressure almost had no effect on S_{BET}. Hydrochar yields increased with N_2 addition (Figure S2), indicating that oligomers in solution were recovered to form hydrochar.[43] EWP-derived hydrochars exhibited low S_{BET} values, indicating that deamination, dehydration, and decarboxylation were enhanced to disrupt agglomeration and form smooth particles. S_{BET} values were lower than those of CL- and LG-derived hydrochar, indicating that probably EWP would cause easier formation of spherical particles compared to CL and LG. The use of PWP as a feedstock led to hydrochars with low surface areas since hydrolysis was inhibited (interfering of LG on CL), leading to low S_{BET} values, in good agreement with previous reports.[13,44] Hence, S_{BET} provided another tool to probe the difference of hydrochar formation mechanisms.

SEM images showed hydrochar morphologies (Figure 5). When CL was used as a feedstock at 260 °C without the addition of MN, a significant agglomeration was found. The presence of MN at 260 °C resulted in the formation of irregular spherical particles, leading to coalescence and generating more irregular spherical particles at prolonged reaction times (10 h). Interestingly, smooth-faced regular spherical particles were observed under pressure (N_2, 10 MPa). From Figure 5A, particles were confirmed to stepwise change to smooth-faced regular spherical particles under more severe HTC reaction conditions. Hollow spherical hydrochar particles are also shown in Figure S8. MN would promote additional −OH and −COOH formation on the surface of the biopolymer, which can benefit dehydration and decarboxylation. Increasing pressure was beneficial for the formation of smooth-faced regular spherical particles. Almost no spherical regular particles could be observed when LG or PWP was employed as a feedstock, while spherical particles were observed for EWP. With the condition getting more severe, more spherical particles can be found together with particle coalescence (Figure S9). According to SEM results, spherical particle formation could be explained via biomass hydrolysis during HTC to form oligomers containing lipophilic and hydrophilic groups, whose interfacial tension decreases stepwise in a crooked manner with the molecular weight increasing. Irregular spherical particles were then formed, with dehydration and decarboxylation occurring; the inner pressure of particles made them change to a spherical shape to form hollow particles. At the same time, particles also coalesced (Figure S10) with dehydration, demethylation, and decarboxylation reactions also taking place on the surface to form smooth-faced hydrochar (particularly promoted with increasing pressures).

XPS results are depicted in Figure S11. C−C/H, C−N, and O—C═O bands can be found as well as pyrrole-N, pyridinic-N, and graphitic-like N. The fraction of different functional groups is summarized in Figure 6. The fraction of C−C/H decreased under harsher reaction conditions, indicating that dehydration was enhanced and the degree of coalification was increased. The high fraction of C−N pointed to the nitrogen

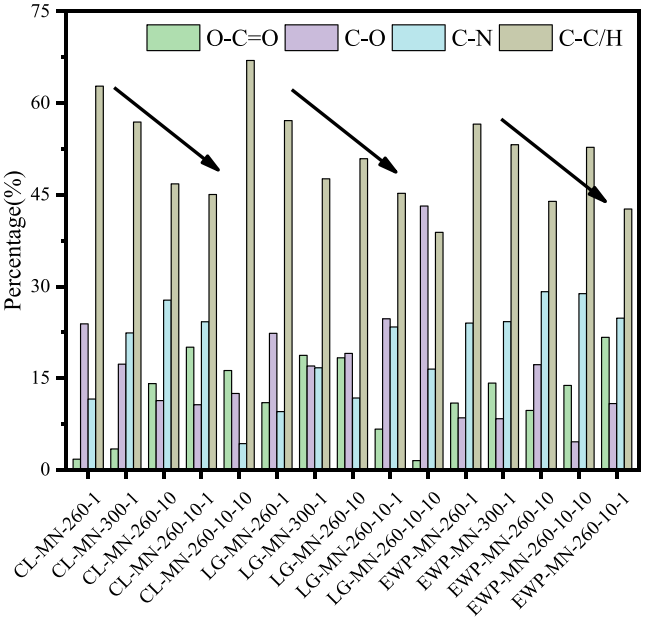

Figure 6. Functional group percentage of hydrochar for XPS under different conditions.

element in NO_3^- transferring to hydrochar. LG-derived hydrochar also possessed C−N bonds, especially pyrrole-N and pyridinic-N, indicating that aromatic rings were probably cleaved by MN. Graphitic-like N has a high fraction in a high degree of coalification. Hence, XPS provided a practical tool to demonstrate the presence of a nitrogen element in NO_3^- transferred to hydrochar.

To analyze the characteristics of the aqueous phase, TOC values of the aqueous phase were measured as listed in Figure S12. The aqueous phase obtained at 300 °C with MN exhibited the lowest TOC value among CL-derived aqueous phases, while that of hydrochar was not the highest among hydrochars, indicating that the original feedstock was partially oxidized to form gases (e.g., CO_2). At the same temperature (260 °C), TOC values increased when MN was added, pointing to the promotion of hydrolysis by MN (transferring to the aqueous phase). TOC values decreased at prolonged reaction times (10 h) or under pressure, indicating the favored transfer of organic matter to the solid. The use of LG as a feedstock provided a different TOC trend as compared to CL. Under severe conditions (pressure, higher temperature, and prolonged times), reducing TOC values were found, pointing to the minor β-O-4 bond that underwent cleavage in LG to release low-molecular-weight compounds. Similar results were obtained for PWP as well as for EWP (but the latter with a high TOC value), implying that most proteins were transferred to the aqueous phase and formed heterocyclic compounds in the aqueous phase during HTC.

Gas chromatography−mass spectrometry (GC−MS) was used to analyze the chemical components present in the aqueous phase as listed in Figure S13. Hydroxymethylfurfural and other furan derivatives were found in CL-MN-200-1, indicating that a low degree of polymerization was present after CL hydrolysis. At the same time, ketones, acids, and amides could also be found, indicating that MN played a key role in the hydrolysis. When KS was used, no N-organic matter could be found, demonstrating that NO_3^- took part in the HTC reaction process to form N-organic matter. A few compounds

https://doi.org/10.1021/acssuschemeng.1c08338
ACS Sustainable Chem. Eng. 2022, 10, 3335−3345

Figure 7. Potential of artificial coal production in China.

could be detected when LG was employed as a feedstock (phenol as the main compound). In other words, the cleavage of LG under HTC with MN was still limited. Vanillin was a classic product derived from β-O-4 bond cleavage. When EWP was used as a feedstock, more compounds could be found, including hydroxymethylfurfural, ketones, acids, and heteroatom compounds. A baseline drift also can be found, perhaps due to partial column bleeding of the stationary phase at higher temperatures. Several strong polar substances are indeed present in the liquid phase that can degrade such a stationary phase.

3.2. Benefits for Developing Artificial Coal-Based Renewable Energy. With the Paris Agreement successfully signed in 2015, China has taken significant actions to tackle climate change issues.[45] Chinese President Xi Jinping announced that "we aim to have CO_2 emissions peak before 2030 and achieve carbon neutrality before 2060".[46] China's government will seize time to formulate an action plan for peaking carbon dioxide emissions before 2030. Artificial coal could be expected to play an important role in the future in the reduction of CO_2 emissions.

The above results demonstrate a feasible approach for the use of widely produced and easily accessed biomass including forestry and agricultural waste to prepare a highly coalified artificial coal. Taking China as an example, the annual output of agricultural straw was about 740 million tons and that of forestry waste was about 200 million tons.[47] A large amount of forestry and agricultural waste would provide a relevant opportunity to substitute the conventional fossil fuel-based energy with artificial coal-based renewable bioenergy. According to the yield of PWP in this paper and considering the yield of agricultural waste,[48] 35% of yield was used to calculate the artificial coal production using agricultural waste as a feedstock (Figure 7). The main crop straw production in 2020 in China is listed in Table S3. Heilongjiang, Henan, Shandong, Anhui, and Jilin provinces could potentially be higher artificial coal production areas, which account for 44.78% total production. At present, coal is still the dominant energy source in China. In 2019, a nationwide energy of about 4.86 billion tce was consumed, 57.7% of which originated from coal.[49] By using artificial coal as an alternative, it would reduce about 282 million tce and decrease the pressure for coal demand and reduce the CO_2 emission. If equal quantities of coal were replaced, 189 million tons of CO_2 emission could be reduced.

4. CONCLUSIONS

This contribution explored the new concept of HTC-to-artificial coal as a potential replacement of widely used coal. Pressure promoted decarboxylation to form hollow smooth-faced regular spherical particles, avoiding agglomeration in the hydrochar. The action of oxidant salts could break down the biopolymer structure to form −OH and −COOH species, following enhanced dehydration and decarboxylation reactions. The produced artificial coal has a high degree of coalification, which may pave the way for a more extended organic waste treatment to bring benefits in emission reduction.

■ ASSOCIATED CONTENT

Supporting Information

The Supporting Information is available free of charge at https://pubs.acs.org/doi/10.1021/acssuschemeng.1c08338.

Experimental details; design of experiments; elemental analysis; Van Krevelen diagrams; hydrochar yields;

https://doi.org/10.1021/acssuschemeng.1c08338
ACS Sustainable Chem. Eng. 2022, 10, 3335−3345

FTIR, XRD, Raman, TG-DTA, and surface area results; SEM, XPS, and TOC results of the aqueous phase; GC–MS results of the organic phase; corresponding supporting figures (PDF)

AUTHOR INFORMATION

Corresponding Authors

Zhi-Xiang Xu – *School of Energy and Power Engineering, Jiangsu University, Zhenjiang 212013, China;* orcid.org/0000-0003-3944-3944; Email: xuzx@ujs.edu.cn

Pei-Gao Duan – *Shaanxi Key Laboratory of Energy Chemical Process Intensification, School of Chemical Engineering and Technology, Xi'an Jiaotong University, Xi'an, Shaanxi 710049, China;* orcid.org/0000-0002-9461-3566; Email: pgduan@xjtu.edu.cn

Rafael Luque – *Departamento de Química Orgánica, Universidad de Córdoba, Cordoba E14014, Spain; Peoples Friendship University of Russia (RUDN University), 117198 Moscow, Russia;* orcid.org/0000-0003-4190-1916; Email: rafael.luque@uco.es

Authors

Xue-Qin Ma – *School of Energy and Power Engineering, Jiangsu University, Zhenjiang 212013, China*

Ya-Qi Shan – *Shaanxi Key Laboratory of Energy Chemical Process Intensification, School of Chemical Engineering and Technology, Xi'an Jiaotong University, Xi'an, Shaanxi 710049, China*

Xun Hu – *School Materials Science and Engineering, University of Jinan, Jinan 250022, China*

Sameh M. Osman – *Chemistry Department, College of Science, King Saud University, Riyadh 11451, Saudi Arabia*

Jun-Jie Liao – *Key Laboratory of Coal Science and Technology, Ministry of Education and State Key Laboratory of Clean and Efficient Coal Utilization, Taiyuan University of Technology, Taiyuan 030024, China;* orcid.org/0000-0003-0983-4469

Complete contact information is available at: https://pubs.acs.org/10.1021/acssuschemeng.1c08338

Notes

The authors declare no competing financial interest.

ACKNOWLEDGMENTS

R.L. gratefully acknowledges Ministerio de Ciencia e Innovacion por funding under project PID2019-109953GB-I00. This paper has been supported by the RUDN University Strategic Academic Leadership Program (R.L.). This paper was funded by the Researchers Supporting Project (number RSP-2021/405), King Saud University, Riyadh, Saudi Arabia. This research was supported by State Key Laboratory of Clean and Efficient Coal Utilization and Key Laboratory of Coal Science and Technology, Ministry of Education (China).

REFERENCES

(1) Scott, V.; Haszeldine, R. S.; Tett, S. F. B.; Oschlies, A. Fossil fuels in a trillion tonne world. *Nat. Clim. Change* **2015**, *5*, 419–423.

(2) Rogelj, J.; den Elzen, M.; Höhne, N.; Fransen, T.; Fekete, H.; Winkler, H.; Schaeffer, R.; Sha, F.; Riahi, K.; Meinshausen, M. Paris Agreement climate proposals need a boost to keep warming well below 2 °C. *Nature* **2016**, *534*, 631–639.

(3) *Statistical Review of World Energy*; www.bp.com/statisticalreview (accessed October 2021).

(4) Staples, M. D.; Malina, R.; Barrett, S. R. H. The limits of bioenergy for mitigating global life-cycle greenhouse gas emissions from fossil fuels. *Nat. Energy* **2017**, *2*, 16202.

(5) Bergius, F. D. *Anwendung hoher Drücke bei chemischen Vorgängen und eineNachbildung des Entstehungsprozesses der Steinkohle*; Halle an der Saale: Germany, 1913.

(6) Shen, Y. F. A review on hydrothermal carbonization of biomass and plastic wastes to energy products. *Biomass Bioenergy* **2020**, *134*, 105479.

(7) Mukherjee, D. K.; Sengupta, A. N.; Choudhury, D. P.; Sanyal, P. K.; Rudra, S. R. Effect of hydrothermal treatment on caking propensity of coal. *Fuel* **1996**, *75*, 477–482.

(8) Titirici, M. M.; Antonietti, M. Chemistry and materials options of sustainable carbon materials made by hydrothermal carbonization. *Chem. Soc. Rev.* **2010**, *39*, 103–116.

(9) Aragón-Briceño, C. I.; Pozarlik, A. K.; Bramer, E. A.; Niedzwiecki, L.; Pawlak-Kruczek, H.; Brem, G. Hydrothermal carbonization of wet biomass from nitrogen and phosphorus approach: A review. *Renew. Energy* **2021**, *171*, 401–415.

(10) Bardhan, M.; Novera, T. M.; Tabassum, M.; Azharul, M.; Atikul, M.; Hameed, B. H. Co-hydrothermal carbonization of different feedstocks to hydrochar as potential energy for the future world: A review. *J. Cleaner Prod.* **2021**, *298*, 126734.

(11) Titirici, M. M.; White, R. J.; Falco, C.; Sevilla, M. Black perspectives for a green future: hydrothermal carbons for environment protection and energy storage. *Energy Environ. Sci.* **2012**, *5*, 6796–6822.

(12) Wikberg, H.; Ohra-aho, T.; Pileidis, F.; Titirici, M. M. Structural and morphological changes in kraft lignin during hydrothermal carbonization. *ACS Sustainable Chem. Eng.* **2015**, *3*, 2737–2745.

(13) Yao, L.; Yang, H.; Yoo, C. G.; Chen, C.; Meng, X.; Dai, J.; Yang, C.; Yu, J.; Ragauskas, A. J.; Chen, X. A mechanistic study of cellulase adsorption onto lignin. *Green Chem.* **2021**, *23*, 333–339.

(14) Reza, M. T.; Rottler, E.; Herklotz, L.; Wirth, B. Hydrothermal carbonization (HTC) of wheat straw: Influence of feedwater pH prepared by acetic acid and potassium hydroxide. *Bioresour. Technol.* **2015**, *182*, 336–344.

(15) Xu, Z. X.; Shan, Y. Q.; Zhang, Z.; Deng, X. Q.; Yang, Y.; Luque, R.; Duan, P. G. Hydrothermal carbonization of sewage sludge: effect of inorganic salts on hydrochar's physicochemical properties. *Green Chem.* **2020**, *22*, 7010–7022.

(16) Wang, T.; Zhai, Y.; Zhu, Y.; Li, C.; Zeng, G. A review of the hydrothermal carbonization of biomass waste for hydrochar formation: process conditions, fundamentals, and physicochemical properties. *Renewable Sustainable Energy Rev.* **2018**, *90*, 223–247.

(17) Nicolae, S. A.; Au, H.; Modugno, P.; Luo, H.; Szego, A. E.; Qiao, M.; Li, L.; Yin, W.; Heeres, H. J.; Berge, N.; Titirici, M. M. Recent advances in hydrothermal carbonisation: from tailored carbon materials and biochemicals to applications and bioenergy. *Green Chem.* **2020**, *22*, 4747–4800.

(18) Falco, C.; Baccile, N.; Titirici, M. M. Morphological and structural differences between glucose, cellulose and lignocellulosic biomass derived hydrothermal carbons. *Green Chem.* **2011**, *13*, 3273–3281.

(19) Falco, C.; Perez Caballero, F.; Babonneau, F.; Gervais, C.; Laurent, G.; Titirici, M. M.; Baccile, N. Hydrothermal carbon from biomass: structural differences between hydrothermal and pyrolyzed carbons via ^{13}C solid state NMR. *Langmuir* **2011**, *27*, 14460–14471.

(20) Zhang, S.; Sheng, K.; Yan, W.; Liu, J.; Shuang, E.; Yang, M.; Zhang, X. Bamboo derived hydrochar microspheres fabricated by acid-assisted hydrothermal carbonization. *Chemosphere* **2021**, *263*, 128093.

(21) Qi, R.; Xu, Z.; Zhou, Y.; Zhang, D.; Sun, Z.; Chen, W.; Xiong, M. Clean solid fuel produced from cotton textiles waste through hydrothermal carbonization with $FeCl_3$: Upgrading the fuel quality and combustion characteristics. *Energy* **2021**, *214*, 118926.

(22) Orem, W. H.; Neuzil, S. G.; Lerch, H. E.; Cecil, C. B. Experimental early-stage coalification of a peat sample and a peatified wood sample from Indonesia. *Org. Geochem.* **1996**, *24*, 111−125.
(23) Mursito, A. T.; Hirajima, T.; Sasaki, K. Upgrading and dewatering of raw tropical peat by hydrothermal treatment. *Fuel* **2010**, *89*, 635−641.
(24) Prado, R.; Brandt, A.; Erdocia, X.; Hallet, J.; Welton, T.; Labidi, J. Lignin oxidation and depolymerisation in ionic liquids. *Green Chem.* **2016**, *18*, 834−841.
(25) Xu, Z. X.; Deng, X. Q.; Zhang, S.; Shan, Y. F.; Shan, Y. Q.; Zhang, Z. M.; Luque, R.; Duan, P. G.; Hu, X. Benign-by-design N-doped carbonaceous materials from hydrothermal carbonization of sewage sludge for supercapacitor applications. *Green Chem.* **2020**, *22*, 3885−3895.
(26) Xu, Z. X.; Song, H.; Li, P. J.; He, Z. X.; Wang, Q.; Wang, K.; Duan, P. G. Hydrothermal carbonization of sewage sludge: effect of aqueous phase recycling. *Chem. Eng. J.* **2020**, *387*, 123410.
(27) Roman, S.; Nabaris, J. M. V.; Ledesma, B.; Gonzalez, J. F.; Laginhas, C.; Titirici, M. M. Production of low-cost adsorbents with tunable surface chemistry by conjunction of hydrothermal carbonization and activation processes. *Microporous Mesoporous Mater.* **2013**, *165*, 127−133.
(28) Liu, J.; Zhang, S.; Jin, C.; Shuang, E.; Sheng, K.; Zhang, X. Effect of swelling pretreatment on properties of cellulose-based hydrochar. *ACS Sustainable Chem. Eng.* **2019**, *7*, 10821−10829.
(29) Buendia-Kandia, F.; Mauviel, G.; Guedon, E.; Rondags, E.; Petitjean, D.; Dufour, A. Decomposition of cellulose in hot-compressed water: detailed analysis of the products and effect of operating conditions. *Energy Fuel* **2018**, *32*, 4127−4138.
(30) Shen, X. J.; Wen, J. L.; Mei, Q. Q.; Chen, X.; Sun, D.; Yuan, T. Q.; Sun, R. C. Facile fractionation of lignocelluloses by biomass-derived deep eutectic solvent (DES) pretreatment for cellulose enzymatic hydrolysis and lignin valorization. *Green Chem.* **2019**, *21*, 275−283.
(31) Liu, H.; Zhai, D. D.; Wang, M.; Liu, J. S.; Chen, X. Y.; Zhang, Z. J. Urea-modified phenol-formaldehyde resins for the template-assisted synthesis of nitrogen-doped carbon nanosheets as electrode material for supercapacitors. *ChemElectroChem* **2019**, *6*, 885−891.
(32) Song, D.; Liu, X.; He, X.; Nie, B.; Wang, W. Investigation on the surface electrical characteristics of coal and influencing factors. *Fuel* **2021**, *287*, 119551.
(33) Liang, W.; Yin, Y.; Wang, L.; Chen, L.; Li, H. A new method of preparing anhydrous magnesium carbonate ($MgCO_3$) under high pressure and its thermal property. *J. Alloys Compd.* **2017**, *702*, 346−351.
(34) Jayaramulu, K.; Dubal, D. P.; Nagar, B.; Ranc, V.; Tomanec, O.; Petr, M.; Datta, K. K. R.; Zboril, R.; Gómez-Romero, P.; Fischer, R. A. Ultrathin hierarchical porous carbon nanosheets for high-performance supercapacitors and redox electrolyte energy storage. *Adv. Mater.* **2018**, *30*, 1705789.
(35) Brown, A. B.; Tompsett, G. A.; Partopour, B.; Deskins, N. A.; Timko, M. T. Hydrochar structural determination from artifact-free Raman analysis. *Carbon* **2020**, *167*, 378−387.
(36) Xu, Z. X.; Song, H.; Zhang, S.; Tong, S. Q.; He, Z. X.; Wang, Q.; Li, B.; Hu, X. Co-hydrothermal carbonization of digested sewage sludge and cow dung biogas residue: Investigation of the reaction characteristics. *Energy* **2019**, *187*, 115972.
(37) Tian, H.; Jiao, H.; Cai, J.; Wang, J.; Yang, Y.; Bridgwater, A. V. Co-pyrolysis of Miscanthus Sacchariflorus and coals: A systematic study on the synergies in thermal decomposition, kinetics and vapour phase products. *Fuel* **2020**, *262*, 116603.
(38) Kang, S.; Li, X.; Fan, J.; Chang, J. Characterization of hydrochars produced by hydrothermal carbonization of lignin, cellulose, D-xylose, and wood meal. *Ind. Eng. Chem. Res.* **2012**, *51*, 9023−9031.
(39) Cao, X.; Ro, K. S.; Chappell, M.; Li, Y.; Mao, J. Chemical suctures of sine-mnure chars produced under different carbonization conditions investigated by advanced solid-state ^{13}C nuclear magnetic resonance (NMR) spectroscopy. *Energy Fuel* **2011**, *25*, 388−397.
(40) Baccile, N.; Laurent, G.; Bahonneau, F.; Fayon, F.; Titirici, M. M.; Antonietti, M. Structural characterization of hydrothermal carbon spheres by advanced solid-state MAS ^{13}C NMR investigations. *J. Phys. Chem. C* **2009**, *113*, 9644−9654.
(41) Castro-Díaz, M.; Uguna, C. N.; Florentino, L.; Díaz-Faes, E.; Stevens, L. A.; Barriocanal, C.; Snape, C. E. Evaluation of hydrochars from lignin hydrous pyrolysis to produce biocokes after carbonization. *J. Anal. Appl. Pyrolysis* **2017**, *124*, 742−751.
(42) Sheng, K.; Zhang, S.; Liu, J.; E, S.; Jin, C.; Xu, Z.; Zhang, X. Hydrothermal carbonization of cellulose and xylan into hydrochars and application on glucose isomerization. *J. Cleaner Prod.* **2019**, *237*, 117831.
(43) Zhao, Y.; Tian, Y.; Zhou, H.; Tian, Y. Hydrothermal conversion of black liquor to phenolics and hydrochar: Characterization, application and comparison with lignin. *Fuel* **2020**, *280*, 118651.
(44) Mäkelä, M.; Volpe, M.; Volpe, R.; Fiori, L.; Dahl, O. Spatially resolved spectral determination of polysaccharides in hydrothermally carbonized biomass. *Green Chem.* **2018**, *20*, 1114−1120.
(45) UNFCCC *Enhanced actions on climate change: China's intended nationally determined contributions*; NDRC, 2015.
(46) *General Assembly*; https://journal.un.org/en/meeting/officials/e6d6ab5e-c0de-ea11-9114-0050569e8b67/2020-09-22.
(47) Cao, L.; Zhang, C.; Chen, H.; Tsang, D. C. W.; Luo, G.; Zhang, S.; Chen, J. Hydrothermal liquefaction of agricultural and forestry wastes: state-of-the-art review and future prospects. *Bioresour. Technol.* **2017**, *245*, 1184−1193.
(48) Cheng, B. H.; Huang, B. C.; Zhang, R.; Chen, Y. L.; Jiang, S. F.; Lu, Y.; Zhang, X. S.; Jiang, H.; Yu, H. Q. Bio-coal: A renewable and massively producible fuel from lignocellulosic biomass. *Sci. Adv.* **2020**, *6*, No. eaay0748.
(49) National Bureau of Statistics *China Statistical Yearbook*; China Statistics Press, 2020 [in Chinese].

https://doi.org/10.1021/acssuschemeng.1c08338
ACS Sustainable Chem. Eng. 2022, 10, 3335−3345